Benchmark Measurements of the Ionization Balance of Non-Local-Thermodynamic-Equilibrium Gold Plasmas

R. F. Heeter, S. B. Hansen, K. B. Fournier, M. E. Foord, D. H. Froula, A. J. Mackinnon, M. J. May, M. B. Schneider, and B. K. F. Young

Lawrence Livermore National Laboratory, P.O. Box 808, L-473, Livermore, California 94550, USA

(Received 31 May 2007; published 8 November 2007)

We present a series of benchmark measurements of the ionization balance of well-characterized gold plasmas with and without external radiation fields at electron densities near 10^{21} cm^{-3} and electron temperatures spanning the range 0.8 to 2.4 keV. We have analyzed time- and space-resolved M-shell gold emission spectra using a sophisticated collisional-radiative model with hybrid level structure, finding average ion charges $\langle Z \rangle$ ranging from 42 to 50. At the lower temperatures, the spectra exhibit significant sensitivity to external radiation fields and include emission features from complex N-shell ions. The measured spectra and inferred $\langle Z \rangle$ provide a stringent test for non-local-thermodynamic-equilibrium models of complex high-Z ions.

DOI: 10.1103/PhysRevLett.99.195001 PACS numbers: 52.25.Jm, 32.30.Rj, 52.25.Os, 52.70.La

Understanding the atomic physics and plasma processes involved in the x-ray emission and absorption of complex ions is a critical component of predictive modeling for high-Z, high-energy-density (HED) plasmas. For applications such as laser-driven inertial confinement fusion (ICF), which has come to rely on high-Z hohlraums to efficiently symmetrize and transfer energy from the laser driver to a target capsule [1], there is particular interest in the atomic and radiation physics near the critical density for optical laser light. At such densities, the simplifying assumption of local thermodynamic equilibrium (LTE) is not valid and reliable non-LTE calculations are required. These calculations are, however, notoriously difficult, as dramatically illustrated at the first non-LTE code comparison workshop [2], where contributed predictions for the average ionization of gold spanned more than 20 charge states. Benchmark laser-plasma measurements at NOVA found average gold charge states $\langle Z \rangle$ near 50 for electron temperatures T_e of 2–2.6 keV and densities n_e near 10^{21} cm^{-3} [3,4]. Coronal-limit measurements at the Livermore electron beam ion trap (EBIT) found $\langle Z \rangle$ near 47 at $T_e = 2.5$ keV and $n_e = 10^{12}$ cm^{-3} [5]. These measurements stimulated significant efforts to advance non-LTE modeling capabilities: the agreement among codes at subsequent workshops improved to within ≈ 10 charge states [6,7] due largely to increasing emphasis on dielectronic recombination [5] and model completeness [8,9]. The most recent non-LTE code comparison workshop [10] saw good agreement among codes near closed-shell ions for a variety of test cases, but disagreement up to 10 charge states for open-shell high-Z ions persists. Since the existing laser-plasma benchmark values for Au $\langle Z \rangle$ lie near the stable Ni-like ion Au^{51+} in a temperature regime where achievable external radiation fields ($T_r \approx 200$ eV) have little influence on $\langle Z \rangle$, they provide neither a stringent test of non-LTE codes in the most difficult regime nor clear information on the response of high-Z plasmas to external radiation. And although the low-density EBIT measurement lies well into the N shell, it does not access the multiply excited configurations that play an important role in collisional-radiative kinetics at the densities most relevant to predictive modeling of energy transfer and radiation flow in ICF plasmas. The present work extends the benchmark NOVA data to lower electron temperatures, where complex N-shell ions dominate the charge state distribution and the plasma is sensitive to a moderate T_r.

The experiments were performed at the OMEGA laser (Laboratory for Laser Energetics, University of Rochester), where beams of 351 nm light at intensities $I = 1 - 7 \times 10^{14}$ W/cm^2 irradiated both faces of thin disk targets composed of a 200 μm-diameter, 0.5 μm thick sample layer (Au or comixed Au + K:Cl) embedded within a 400 μm-diameter, 10.8 μm thick tamper disk (Be). The laser deposited 0.26–1.5 kJ over 4 ns in a fixed laser spot size of 280 μm (geometric). Some of the targets were, in addition, heated indirectly by placement inside 1.6×1.2 mm tungsten-coated hohlraums, whose surface subtended 61% of the 4π solid angle surrounding the

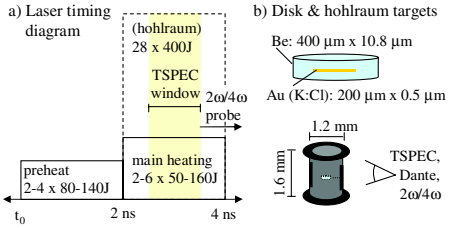

FIG. 1 (color online). (a) Diagram showing the timing of direct disk preheat, main disk heating, hohlraum heating, and TSPEC and Thomson scattering measurements. The number and energy of the heating beams are also given; ranges indicate variations in the experimental series. (b) Target diagrams and dimensions and the orientation of diagnostics.

sample. Figure 1 gives the laser schematics of the targets and the timing of direct and hohlraum laser heating. Under these conditions, the tamped Au sample was predicted to expand by $t = 2.8$ ns into a hot plasma with density uniform to 10% and temperature uniform to 5% [3].

The plasma conditions were diagnosed using a complete set of four independent measurements [11,12]. First, Thomson scattering (TS) diagnostics with 50 J probe beams at either 2ω or 4ω [13] were fielded on a subset of the experiments, giving measured T_e data (averaged across a 200 μm diameter region centered within the Au volume) that follow roughly the intensity scaling predicted by Lindl [1] as shown in Fig. 2. The best fit to the TS data, $T_e(\mathrm{keV}) = 0.67 \times [I/10^{14}\ \mathrm{W/cm^2}]^{2/3}$, was used to determine T_e for all of the experimental measurements. Second, time-gated (0.2 ns), spatially resolved, and relatively calibrated x-ray spectral data were obtained with spectral resolution of $E/\Delta E \approx 240$ and spatial resolution of 50 μm. This spectrometer measured the M-shell Au emission spectra, provided additional temperature data from the simultaneous K-shell emission spectra of the comixed K and Cl ions, and, viewing the samples nearly edge-on (79.2° to the surface normal), also measured the axial expansion of the samples. Third, gated pinhole images showed minimal target expansion in the radial direction [11]); the axial expansion data then determined the ion density to within 20% at the time of the Au, K, and Cl spectroscopic measurements (t_m). Assuming charge neutrality, the electron density was inferred from the measured average ion charge for Au (and K:Cl when present). Analysis of multiple time-gated spectra from each shot confirms the axial spatial uniformity of the Au plasma and sets the limit of density variation due to expansion during the 0.2 ns measurements to be less than 35%. Finally, for the samples with additional hohlraum heating, the Dante instrument [14], an absolutely calibrated multi-channel filtered diode array, measured the hohlraum radiation temperature to be 185 eV at t_m.

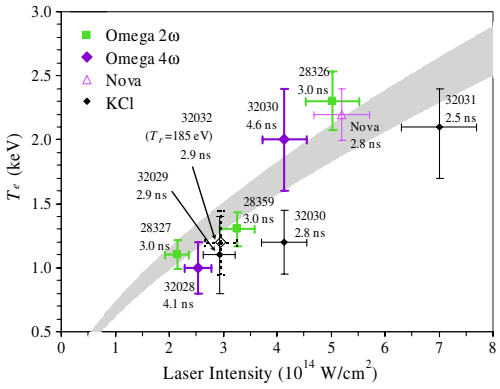

FIG. 2 (color online). Electron temperature measurements from Thomson scattering and spectroscopy of K:Cl tracers at various laser intensities, along with shot numbers and measurement times. The gray region is the best fit of the TS data to an $I^{2/3}$ intensity scaling with width corresponding to 10% experimental uncertainty in I. The measured T_e of the 5.2×10^{14} W/cm^2 case is in good agreement with the previous Nova experiment [3].

The K-shell emission spectra from the Au + K:Cl comix targets were analyzed with collisional-radiative models [15] based on data from the flexible atomic code (FAC) [16]. The K-shell K and Cl models include singly excited states up to $n = 6$ and doubly excited states up to $n = 4$ for H- through Be-like ions, with self-consistent opacity effects modeled using the escape factor formalism for a 200 μm slab and the external radiation field in the hohlraum-enclosed measurements modeled by a 185 eV blackbody with a dilution factor of 0.61. Since equilibration between He- and H-like K and Cl ions can take several ns at the measured electron densities, time-dependent effects are approximated by setting H-like ion populations to zero at the onset of the main heating beams ($t = 2$ ns) and solving for time-dependent ion populations using rates determined by the measured n_e and T_r at t_m at various constant T_e. The K:Cl temperature is diagnosed by finding the best fit to the time-gated experimental data of time-dependent synthetic spectra integrated over $t_m \pm 100$ ps. These temperatures are plotted along with the TS measurements in Fig. 2 with error bars determined by the spread of the best-fit temperatures to three diagnostic line ratios. The spectroscopic temperatures from $t_m = 2.5$–2.9 ns tend to fall below the temperatures measured by Thomson scattering (3.0–4.6 ns), suggesting that T_e may be increasing at the time of the spectroscopic measurements, a suggestion confirmed by analysis of K-shell emission from later time frames, which indicate ≈10% temperature increases over 0.3–0.5 ns. Temperatures diagnosed using steady-state K-shell diagnostics would be ≈10% lower than those found with the time-dependent analysis.

To better understand the time dependence of the sample expansion and temperature, we have performed a two-dimensional radiation-hydrodynamic simulation with the LASNEX code [17] for one of the of the Au:KCl comix samples (shot 32030). The laser power was delivered to both faces of the target by cone 1 OMEGA beams incident to the target faces at an angle of 21.4° with respect to the sample axis and absorbed via inverse bremsstrahlung; each face of the target sees two preheat beams with 135 J/beam and three main heating beams with 68 J/beam. The simulation gives densities consistent with the experimental measurements and temperatures of 1.15 keV at the end of the 2 ns preheat pulse and 1.25 keV at the time of the spectroscopic measurement $t_m = 2.8$ ns. This variation in T_e is gentle enough, and the equilibration between the dominant Au ions is rapid enough (<0.1 ns), that we may consider the Au ions to be in steady state during the 0.2 ns duration of the spectroscopic measurements.

To determine the average ion charge $\langle Z \rangle$ of the measured Au spectra, we have constructed a hybrid fine-structure/UTA model [18] of Fe- to Sr-like Au based on data from the FAC code [16]. For $(n)^N$ denoting a superconfiguration with occupation number N and principle quantum number

n, the modeled level structure for Fe- to Ni-like Au ions includes all possible configurations in $(1)^2(2)^8(3)^N$ and $(1)^2(2)^8(3)^{N-1}(n)^1$ with $n = 4$–7. The Ni-like ion includes additionally all possible double excitations in the superconfiguration $(1)^2(2)^8(3)^{16}(4)^1(n)^1$ with $n = 4$–5 to account for prominent $3d^8 4\ell 5f - 3d^9 4\ell$ emission features to the blue of the dominant $3d^9 5f - 3d^{10}$ lines [3,19]. The Zn- through Ge-like ions include all possible configurations in $(1)^2(2)^8(3)^{18}(4)^N$, $(1)^2(2)^8(3)^{18}(4)^{N-1}(n)^1$ with $n = 4$–7, and $(1)^2(2)^8(3)^{17}(4)^N(n)^1$ with $n = 4$–6. As- through Sr-like ions are modeled with similar structure but exclude configurations with more than one $4f$ electron to keep the model tractable. For all ions, a "coronal" subset of the relativistic configurations, defined as those configurations accessible through single-electron excitation from the ground configuration, is replaced by detailed fine-structure levels to form the hybrid model. Transitions among these fine-structure levels include configuration interaction effects and thus have more accurate energies and strengths than the unresolved transition arrays (UTAs) they replace in the hybrid model; this accuracy is extended to the remaining UTAs in each ion by applying energy shifts and oscillator strength factors from the fine-structure transitions to all $n\ell j - n'\ell' j'$ transitions. To determine the steady-state populations in the resultant set of 2.1×10^6 mixed levels, we construct the full collisional-radiative rate matrix and follow the averaging procedure detailed in Ref. [18] to obtain and solve a smaller rate matrix for an averaged model. We then restore the full model, finding the populations of the averaged levels from stored configuration-to-level rates in a procedure roughly based on Ref. [20]. The spectra obtained from the hybrid model are in very good agreement with spectra from a restricted, tractable fine-structure model of Co- to Cu-like ions. Since a similarly complete fine-structure model of Fe- to Sr-like ions would have more than 10^{10} levels, the computational efficiencies of the hybrid scheme are essential.

Determining the experimental charge state distribution (CSD) by fitting the calculated emission from each ion to the experimental data is not trivial: each ion contributes 3–6 significant features to the 2.9–3.6 keV spectral range and there is significant overlap between the emission from different ions. We have thus employed a genetic algorithm [15,21] to search a wide range of possible CSDs seeking the best fit to 27 intensity points in the 2.9–3.6 keV spectral range. We obtain an initial CSD by fitting the experimental data using emission features calculated at the measured n_e, T_e, and T_r. These fits rely on the hybrid model's predictions for the CSD, since the spectra from individual ions are influenced by opacity and the relative importance of different population mechanisms. Although the hybrid model predicts $\langle Z \rangle$ within the final error bars for most shots, its performance deteriorates near the edges of the modeled ion range. To ensure self-consistency in the reported CSDs, we adjust the rates between ground states to enforce the initial best-fit CSD, recalculate the emission spectra, and fit the data a second time. We find that, as in Ref. [3], opacity effects reduce the intensities of the 5–3 emission features by as much as ≈20%. The self-consistent CSD has a larger effect on the emission than variations of 10% in temperature or density with a fixed CSD and is most important at low temperatures where dielectronic rates tend to dominate over direct collisional excitation. Error bars for the fractional ion populations are the sum of the standard errors from three sources: (i) fit uniqueness as determined by five different trials of the genetic algorithm, (ii) a ±50% uncertainty in the emission intensity per ion on either side of the Ge-/As-like ion divide associated with the exclusion of states with more than one $4f$ electron in As- through Sr-like ions, and (iii) differences in the first- and second-pass CSDs which reflect uncertainty in opacity effects and population mechanisms. Error bars on the final average $\langle Z \rangle$ incorporate all three standard errors at fixed conditions. Since equilibration times among the dominant

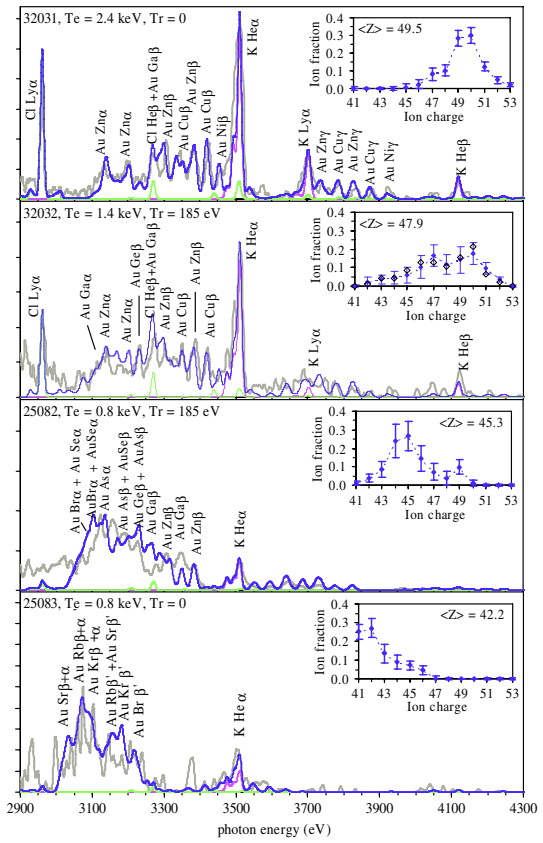

FIG. 3 (color online). Experimental data (thick gray lines) overlaid with modeled emission (thin blue lines) which include diagnostic K-shell K and Cl spectra (magenta and green lines, respectively) and the best-fit M-shell Au emission obtained using the inset charge state distributions. The CSD from shot 25 086, given by hollow diamonds in the inset of shot 32 082, demonstrates reproducibility. The dominant components of selected M-shell emission features are labeled by parent ion, isoelectronic sequence, and transition type: $\alpha = 4p_{3/2} - 3s_{1/2}$, $\alpha' = 4d_{3/2} - 3p_{1/2}$, $\beta = 5f_{7/2} - 3d_{5/2}$, $\beta' = 5f_{5/2} - 3d_{3/2}$, $\gamma = 6f_{7/2} - 3d_{5/2}$, and $\gamma' = 6f_{5/2} - 3d_{3/2}$. The feature at 3375 eV in shot 25 083 is an experimental artifact.

TABLE I. Laser intensities and plasma conditions at the time of the M-band Au measurements (t_m), inferred average Au ion charge, and width σ_Z of the CSD. The tabulated T_e have error bars of +15% and −25% due to uncertainties in the laser intensities, the use of a scaled fit to Thomson scattering data for T_e, and the possibility that T_e was below its intensity-scaled value at t_m.

Shot	$I(10^{14}$ W/cm$^2)$	T_e (keV)	T_r (eV)	$n_e(10^{20}$ cm$^{-3})$	t_m (ns)	Au $\langle Z\rangle$	σ_Z
Ref. [4]	-	2.6	190	14	1.6	50.5 ± 1.0	2.0
32 031	7.0	2.4	0	6	2.5	49.5 ± 0.5	2.1
25 080	5.2	2.0	185	6	2.6	49.6 ± 0.5	1.1
Ref. [3]	5.2	2.0	0	6	2.8	49.3 ± 0.5	1.5
32 030	4.1	1.7	0	7	2.8	48.8 ± 0.7	2.6
32 032	2.9	1.4	185	10	2.9	47.9 ± 1.4	5.8
25 086	2.9	1.4	185	9	2.7	47.8 ± 1.4	5.4
32 029	2.9	1.4	0	10	2.9	46.8 ± 1.2	5.0
25 082	1.4	0.8	185	11	2.6	45.3 ± 1.5	3.6
25 083	1.4	0.8	0	7	2.7	42.2 ± 1.2	2.6

Au ions are shorter than 0.1 ns, there is no additional uncertainty in $\langle Z\rangle$ due to time-dependent effects.

Figure 3 shows experimental emission with the best-fit modeled spectra. Each M-shell ion contributes two $5f - 3d$ features separated by $\approx$ 80 eV and several $4p - 3s$ and $4d - 3p$ features at lower energies. With decreasing ion charge, the $5f - 3d$ features shift to lower energies by $\approx$40 eV per ion and the separation between 5-3 and 4-3 features decreases. The inferred charge state distributions are inset; the good agreement in the CSDs of the similar shots 32 032 and 25 086 (hollow diamonds in the second panel) indicates good reproducibility in the experimental data and fitting procedure. The low-temperature, $T_r = 0$ case assumes a population fraction of 0.15 in the ions with $Z \leq 40$ that were not modeled. The complete results of the fitting to all experimental spectra are summarized in Table I. The effect of the external radiation field is most significant at low T_e, where collisional excitation and ionization rates are not dramatically larger than photoexcitation and photoionization rates. The CSD widths tend to be smallest when $\langle Z\rangle$ is near a closed-shell ion.

These benchmark measurements of $\langle Z\rangle$ and M-shell emission spectra across a wide range of T_e and T_r can be used to test and verify non-LTE models of complex, high-Z ions. Improved understanding of the internal energy, radiative properties, and interaction with external radiation fields of non-LTE high-Z ions could have a significant impact on ICF science. The presented analysis also demonstrates the efficacy of a hybrid model for providing spectroscopic-quality emission from N-shell ions for which UTA models would be inaccurate and fine-structure models would be intractable.

We thank the crew of the Omega laser at the University of Rochester Laboratory for Laser Energetics for expertly executing these experiments and Jacques Bauche and Claire Bauche-Arnoult for valuable discussions on non-LTE hybrid models. This work was performed under the auspices of the U. S. Department of Energy by Lawrence Livermore National Laboratory in part under Contract W-7405-Eng-48 and in part under Contract DE-AC52-07NA27344.

[1] J. Lindl, Phys. Plasmas **2**, 3933 (1995). (Scaling law given on p. 3995).
[2] R. W. Lee, J. K. Nash, and Y. Ralchenko, J. Quant. Spectrosc. Radiat. Transfer **58**, 737 (1997).
[3] M. E. Foord, S. H. Glenzer, R. S. Thoe, K. L. Wong, K. B. Fournier, B. G. Wilson, and P. T. Springer, Phys. Rev. Lett. **85**, 992 (2000); M. E. Foord *et al.*, J. Quant. Spectrosc. Radiat. Transfer **65**, 231 (2000).
[4] S. H. Glenzer, K. B. Fournier, B. G. Wilson, R. W. Lee, and L. J. Suter, Phys. Rev. Lett. **87**, 045002 (2001).
[5] K. L. Wong, M. J. May, P. Beiersdorfer, K. B. Fournier, B. Wilson, G. V. Brown, P. Springer, P. A. Neill, and C. L. Harris, Phys. Rev. Lett. **90**, 235001 (2003).
[6] C. Bowen, A. Decoster, C. J. Fontes, K. B. Fournier, O. Peyrusse, and Yu. V. Ralchenko, J. Quant. Spectrosc. Radiat. Transfer **81**, 71 (2003).
[7] C. Bowen, R. W. Lee, and Yu. Ralchenko, J. Quant. Spectrosc. Radiat. Transfer **99**, 102 (2006).
[8] O. Peyrusse, C. Bauche-Arnoult, and J. Bauche, J. Phys. B **38**, L137 (2005).
[9] Z. Wu, J. Pang, and J. Yan, J. Quant. Spectrosc. Radiat. Transfer **102**, 402 (2006).
[10] J. G. Rubiano, R. Florido, C. Bowen, R. W. Lee, and Yu. Ralchenko, High Energy Density Phys. **3**, 225 (2007).
[11] R. F. Heeter *et al.*, *Proceedings of Inertial Fusion Sciences and Applications 2003* [American Nuc. Soc., LaGrange Park, IL (to be published)].
[12] R. F. Heeter *et al.*, *Proceedings of Atomic Processes in Plasmas 2004*, edited by J. S. Cohen, S. Mazevet, and D. P. Kilcrease (AIP, Melville NY, 2004), p. 103.
[13] S. H. Glenzer *et al.*, Phys. Rev. Lett. **77**, 1496 (1996).
[14] H. N. Kornblum, R. L. Kauffman, and J. A. Smith, Rev. Sci. Instrum. **57**, 2179 (1986).
[15] S. B. Hansen, Ph.D. thesis, University of Nevada, Reno, 2003.
[16] M. F. Gu, Astrophys. J. **582**, 1241 (2003).
[17] G. Zimmerman and W. Kruer, Comments Plasma Phys. Control. Fusion **2**, 51 (1975).
[18] S. B. Hansen, J. Bauche, C. Bauche-Arnoult, and M. F. Gu, High Energy Density Phys. **3**, 109 (2007).
[19] C. Bauche-Arnoult *et al.*, Phys. Rev. A **33**, 791 (1986).
[20] F. B. Rosmej, Europhys. Lett. **76**, 1081 (2006).
[21] I. E. Golovkin, R. C. Mancini, S. J. Luis, R. W. Lee, and L. Klein, J. Quant. Spectrosc. Radiat. Transfer **75**, 625 (2002).